ELSEVIER

Journal of Biomechanics 40 (2007) 125–136

JOURNAL OF BIOMECHANICS

www.elsevier.com/locate/jbiomech
www.JBiomech.com

Computational and experimental models of the human torso for non-penetrating ballistic impact

J.C. Roberts[a,b,*], A.C. Merkle[a], P.J. Biermann[a], E.E. Ward[a], B.G. Carkhuff[a], R.P. Cain[a], J.V. O'Connor[c]

[a]*Applied Physics Laboratory, The Johns Hopkins University, Laurel, MD 20723-6099, USA*
[b]*Department of Mechanical Engineering, The Johns Hopkins University, Baltimore, MD 21218, USA*
[c]*Thoracic and Vascular Surgery, R. Adams Cowley Shock Trauma Center, University of Maryland Medical System, Baltimore, MD 21201, USA*

Accepted 9 November 2005

Abstract

Both computational finite element and experimental models of the human torso have been developed for ballistic impact testing. The human torso finite element model (HTFEM), including the thoracic skeletal structure and organs, was created in the finite element code LS-DYNA. The skeletal structure was assumed to be linear-elastic while all internal organs were modeled as viscoelastic. A physical human surrogate torso model (HSTM) was developed using biosimulant materials and the same anthropometry as the HTFEM. The HSTM response to impact was recorded with piezoresistive pressure sensors molded into the heart, liver and stomach and an accelerometer attached to the sternum. For experimentation, the HSTM was outfitted with National Institute of Justice (NIJ) Level I, IIa, II and IIIa soft armor vests. Twenty-six ballistic tests targeting the HSTM heart and liver were conducted with 22 caliber ammunition at a velocity of 329 m/s and 9 mm ammunition at velocities of 332, 358 and 430 m/s. The HSTM pressure response repeatability was found to vary by less than 10% for similar impact conditions. A comparison of the HSTM and HTFEM response showed similar pressure profiles and less than 35% peak pressure difference for organs near the ballistic impact point. Furthermore, the peak sternum accelerations of the HSTM and HTFEM varied by less than 10% for impacts over the sternum. These models provide comparative tools for determining the thoracic response to ballistic impact and could be used to evaluate soft body armor design and efficacy, determine thoracic injury mechanisms and assist with injury prevention.

Keywords: Non-penetrating ballistic impact; Finite element modeling; Human torso; Experimental testing

1. Introduction

1.1. Computational models

One of the first finite element models (FEMs) of the thorax was created by Roberts and Chen (1970). In this model, linear elastic material properties were used (neglecting soft tissue properties) and only static loads were imposed on the sternum. In subsequent studies, Chen (1973) and Chen and Roberts (1974) used this same model with a dynamic modal synthesis technique. Later, Chen (1978) used a two level "thorax/subsystem" modal synthesis method to expand the baseline model. This model was similar to the previous, but also had the capability of incorporating the visceral subsystem. Sundaram and Feng (1977) formulated two distinct FEMs of the thorax, using half symmetry models to save computing time. The first model consisted of a hollow skeletal cage containing elements representing the thoracolumbar portion of the vertebral column, the sacrum, the coccyx, ribs 1–10 and the sternum. The second model was that of the full thoracic body including muscle and gross internal organs. Linear

*Corresponding author. Department of Mechanical Engineering, The Johns Hopkins University, Baltimore, MD 21218, USA.
Tel.: +1 240 228 3788.
E-mail address: jack.roberts@jhuapl.edu (J.C. Roberts).

0021-9290/$ - see front matter © 2005 Elsevier Ltd. All rights reserved.
doi:10.1016/j.jbiomech.2005.11.003

elastic behavior was assumed for all materials. Stuhmiller et al. (1988) constructed a 3-D FEM of a sheep thorax to respond to blast events. This model was divided into groups of solid elements representing the lungs, omasum, small intestine, rumen, and large intestine. The material was assumed to be linear-viscoelastic.

More recently, Plank et al. (1998) created a FEM of the thorax for frontal impact simulation. This, as well as the earlier model by Plank and Eppinger (1991), contained a much better physical description of the human thorax than previous models as well as a more realistic thoracic skeletal structure. Although the ribs, sternum, spine, muscles, and some cartilaginous ligaments were modeled, the separate internal organs were not. Linear elastic material properties were assumed for all elements except for the interior elements, where a viscoelastic model was used. Wang (1995) constructed a FEM that included the complete musculoskeletal structure as well as internal organs. Viscoelastic properties were used for the organs and elastic properties were assigned to the bone. Jolly and Young (2000) created a FEM that included the skeletal structure with elastic properties and muscle with viscoelastic properties.

1.2. Experimental models

In addition to the use of post-mortem human subjects (PMHS) and animal (pig, sheep, etc.) subjects for testing, a number of test devices have been constructed for ballistic impact. Jönsson et al. (1981, 1988) designed an anthropometric dummy specifically for blast, blunt impact, and missile testing which consisted of wood, water, and plastic. The lungs were constructed of two pieces of cylindrical plastic foam with a total volume approximately equal to that of an adult and were positioned within a water-filled torso. The head was made of wood with airways and pressure transducers corresponding to tympanic membranes. A pressure transducer was also placed in the center of each lung for recording intrathoracic pressures and peak overpressures. The Australian Defence Science and Technology Organisation (DSTO) has developed a torso model designated as AUSMAN made with polyurethane and a stainless-steel rib cage currently used in blast testing with the intent of conducting ballistic tests as well. The Naval Research Laboratory (NRL) has a human torso consisting of type 250A Ordnance Gelatin. At present, it is a rib cage enclosed in a block of gelatin with different density silicone gel material for the lungs. This model can be used with a soft armor vest to identify the pressures and shock waves generated through the gel during a ballistic impact. Lyons et al. (1999) extracted three rib structure sub-units from a BIOSID crash test dummy to create a surrogate for non-penetrating ballistic impact testing. The model consists of ribs, a spine box, damping material, nylon supports for the spine box, and a conductive-plastic position transducer. None of the aforementioned models have a skeletal structure made with the elastic properties of bone or internal organs with viscoelastic properties measured at high (ballistic) strain rates. In addition, none of the physical models have been used in conjunction with a computational FEM that is an exact replica of the physical model.

The purpose of this investigation was to develop both a computational and an experimental model of the human torso for ballistic impact. A 5th percentile male human torso finite element model (HTFEM) was created and includes the skeletal system (ribs, sternum, cartilage, and vertebral column), internal organs (heart, liver, lungs, and stomach), mediastinum, muscle, tissue, and skin. Linear elastic properties were used for bone and viscoelastic properties were used for all internal organs and viscera. A physical human surrogate torso model (HSTM) was developed with the same anthropometry as the HTFEM, and included the previously mentioned skeletal structures and organs. The bones were fabricated to have the tensile properties of human cancellous bone and the organs were formulated of silicone gel. Piezoresistive pressure sensors were placed in the heart, liver and stomach and an accelerometer was mounted to the back of the sternum. The HSTM was tested under ballistic impact conditions and the response was compared with that of the HTFEM exercised under similar conditions.

2. Methods

2.1. Human Torso Finite Element Model (HTFEM)

A model of the human male was obtained from Viewpoint (Draper, UT) in the form of initial graphics exchange specification (IGES) point clouds. Creation of the finite element model of the HTFEM is contained in Roberts et al. (2005) but will be briefly discussed here. Figs. 1a–c shows the HTFEM along with its components. The skeletal structure, organs, and mediastinum were modeled with linear tetrahedral solid elements. The peripheral musculature and skin were modeled as a single entity using membrane elements. The complete model is shown in Fig. 1d. The assembled model was exported to the explicit finite element code LS-DYNA (Liverware Software, Livermore, CA) to be exercised in a dynamic environment. The internal organs do not share nodes and therefore transfer load through defined contact interfaces between the various components. This allows for the definition of a frictionless condition at the boundaries between all organs and between the organs and the skeletal structure. The slip condition was enforced by assigning an extremely low coefficient of friction in the contact definition.

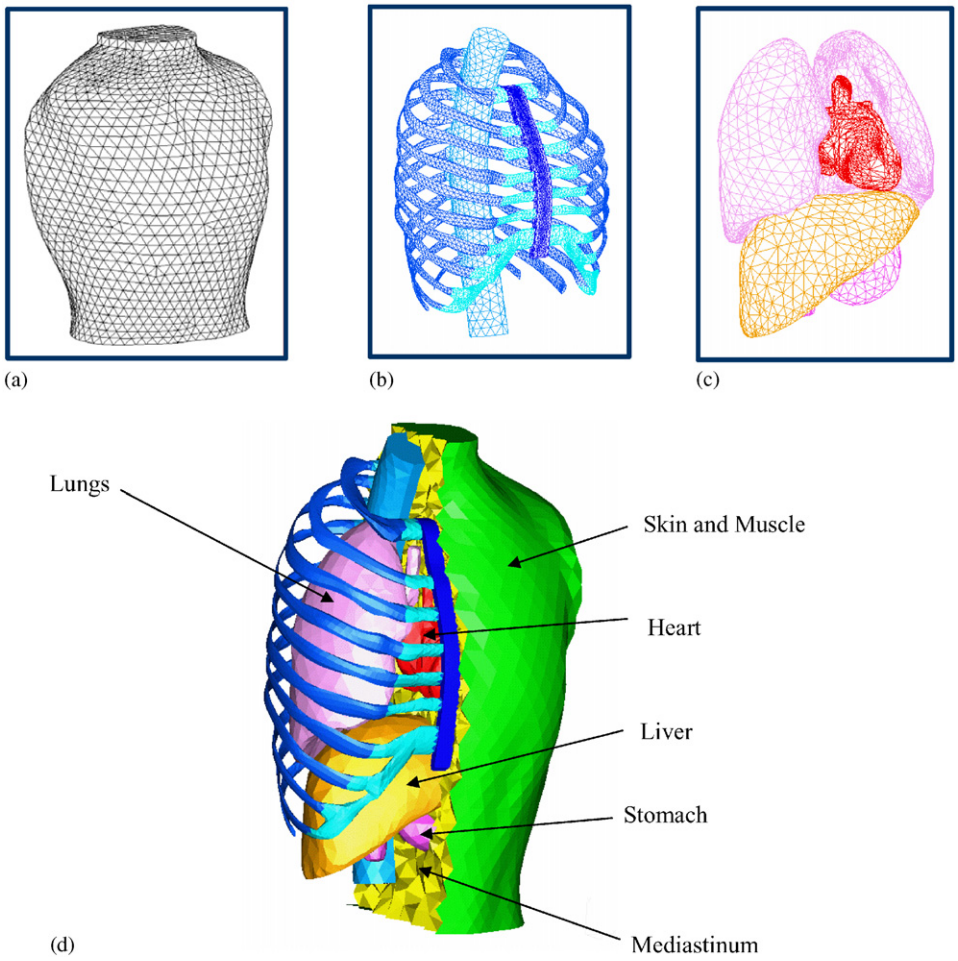

Fig. 1. HTFEM components including: (a) skin/muscles, (b) skeletal structure, and (c) internal organs. The complete model is shown in (d) with part of the skin removed.

The internal organ properties were taken from modified split-Hopkinson bar tests conducted on silicon gel simulants at strain rates up to 1500 1/s by Saraf et al. (2005). The elastic properties for the ribs and sternum were taken from Caruso et al. (2006) while those of the vertebral column were from Wang (1995) and Duck (1990). The element type, number of elements, elastic material properties (Young's modulus—E, Poisson's ratio—v), and viscoelastic material properties (G_0, G_∞, β and bulk modulus—K) for the HTFEM components are shown in Table 1.

Soft armor vests were modeled on the torso with the material thicknesses for National Institute of Justice (NIJ) Level I, II, IIa and IIIa vests of 4.87, 7.88, 9.50 and 10.82 mm, respectively. The Kevlar fabric has an elastic modulus in the warp and fill directions that falls into a low-strain, low-stiffness region which causes a progressive uncrimping of the fabric when deformed, Grosberg (1969). Therefore, the lower modulus of $E = 7.4$ GPa from Johnson et al. (1999) was used in the model.

The impact event used for the simulations included either a 9 mm (8 g) projectile modeled with 358 tetrahedral solid elements or a 22 caliber (2.6 g) projectile modeled with 871 tetrahedral solid elements. The kinematic plastic material model, Material Model 3, was used to model the bullet with plastic deformation during impact to ensure proper energy transfer to the armor and, subsequently, the torso.

2.2. Physical HSTM

Each part of the HSTM was created from the exact geometry used to build the HTFEM, thus creating anatomically identical models. As previously mentioned, both the bulk and shear moduli of the biosimulant organs were taken from modified split-Hopkinson bar tests performed on silicone gels[1] and the elastic modulus for bone was taken from a bone replacement material developed by Caruso et al. (2006) with the properties

[1]Experimentation performed at the Department of Mechanical Engineering at Johns Hopkins University.

Table 1
Element information for the HTFEM, material composition of the HSTM, and the material properties for both the HSTM and HTFEM

	Solid elements in HTFEM	Shell membrane elements in HTFEM	Materials in HSTM	$E^{a,b,c}$ (GPa)	$v^{a,b}$	G_0^d (kPa)	G_∞ (kPa)	K^d (Gpa)	β	$\rho^{a,b}$ (kg/mm^3) $\times 10^{-6}$
Skin/muscles	–	3948	Silicone XP429 (Silicone, Inc, High Point, NC) with fillers added	–	–	200	195	2.9	0.1	1.20
Ribs	15,048	–	Shell Epon 862+, Epi-cure 3274+, TiO_2, calcinated alumina and milled fiberglass, RP-806++	9.5	0.20	–	–	–	–	1.08
Sternum	4919		Shell Epon 862+, Epi-cure 3274+, TiO_2, calcinated alumina and milled fiberglass, RP-806++	9.5	0.25	–	–	–	–	1.25
Vertebral column	8651	–	Shell Epon 862+, Epi-cure 3274+, TiO_2, calcinated alumina and milled fiberglass, RP-806++	0.355	0.26	–	–	–	–	1.33
Cartilage	6238	–	Smooth-on Evergreen 40 (Smooth On, Easton, PA)	0.0025	0.40	–	–	–	–	1.07
Heart	6841	–	Silicone XP429 (Silicone, Inc, High Point, NC) with added filler	–	–	67	65	0.744	0.1	1.00
Lungs	11,262	–	Silicone foam R2370 (Nusil, Carpinteria, CA)	–	–	67	65	0.744	0.1	0.60
Mediastinum and viscera	182,781	–	Silicone XP429 (Silicone, Inc, High Point, NC) with added filler	–	–	200	195	1.03	0.1	2.07
Liver	3377	–	Silicone XP429 (Silicone, Inc, High Point, NC) with added filler	–	–	67	65	0.744	0.1	1.06
Stomach	2314	–	Silicone XP429 (Silicone, Inc, High Point, NC) with added filler	–	–	67	65	0.744	0.1	1.05
Total	241,917	3948								

[a]Duck, F.A. (1990).
[b]Wang, H.C. (1995).
[c]Caruso, K.S. et al. (2006).
[d]Internal generated in modified split-Hopkinson bar at the Johns Hopkins University, Department of Mechanical Engineering. Short-term shear modulus (G_0) data collected at a strain rate of 1500 l/s and bulk modulus data collected at pressures from 50 to 175 Mpa. See Saraf et al. (2005) for details on the experimental set-up.

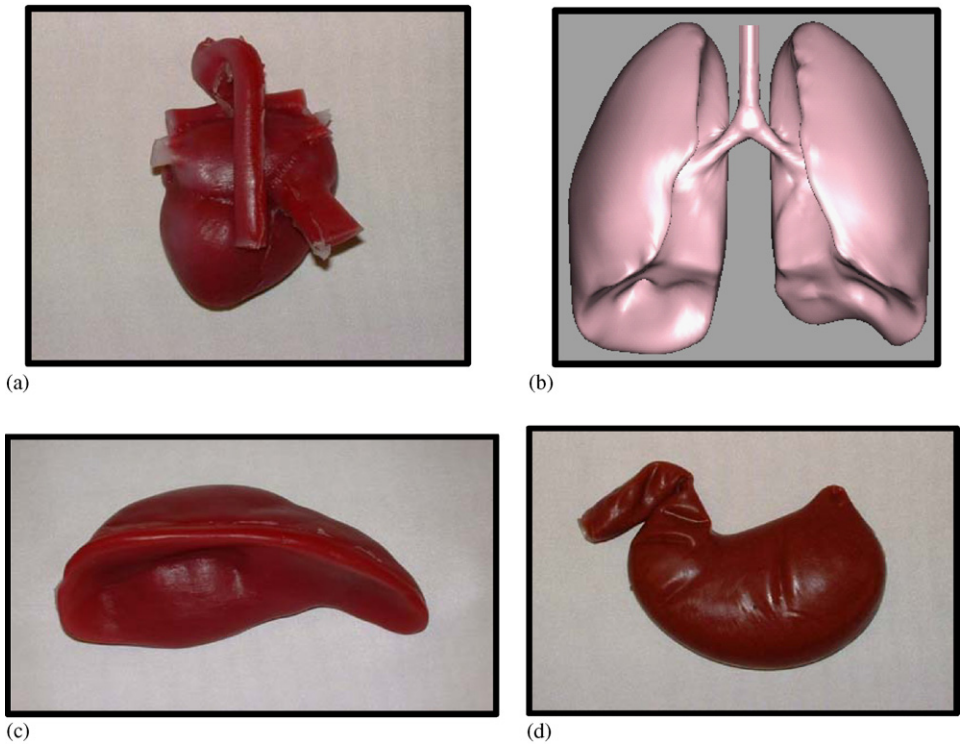

Fig. 2. Completed organs for the HSTM including: (a) heart, (b) lungs, (c) liver, and (d) stomach.

Fig. 3. (a) Skeleton (ribs, sternum, cartilage, and vertebral column) and (b) completed HSTM with muscle and skin.

listed in Table 1. Fig. 2 includes photographs of the final surrogate organs, while Fig. 3 shows the skeleton (ribs, sternum cartilage, and vertebral column) along with the completed HSTM with muscle and skin.

Piezoresistive pressure sensors (Entran Devices, Inc., Fairfield, NJ)[2] were embedded in the heart, liver and

[2]Entran model EPB-B03-5KP.

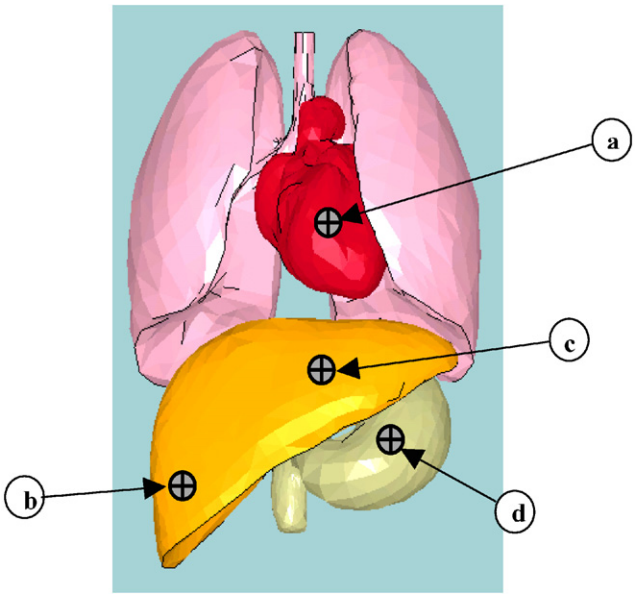

Fig. 4. Location of piezoelectric pressure sensors: (a) middle of the heart, (b) right lobe of the liver, (c) the liver directly below the sternum, and (d) approximately the middle of the stomach. An accelerometer was attached to the sternum at approximately the level of the T6 vertebrae.

stomach (Fig. 4) during molding of these organs. Accelerometers (Endevco Corp., San Juan Capistrano, CA)[3] were bonded to the back of the sternum (vertical position even with T6) and to the vertebral column on the T6 vertebrae. A TDAS Pro data acquisition system (Diversified Technical Systems, Seal Beach, CA) was used to collect data from the pressure sensors and accelerometer at 300 kHz.

The HSTM was evaluated under ballistic impact conditions at the H.P. White Ballistics Laboratory (Street, MD). Tests were performed with 22 caliber (2.6 g) ammunition at a velocity of 329 m/s against a Level I soft armor vest and with 9 mm (8 g) ammunition at velocities of 332, 358 and 430 m/s against Level IIa, II and IIIa soft armor vests, respectively, as determined by NIJ standard 0101.04. The two target locations used on the HSTM (Fig. 5) were the middle of the sternum body anterior to the T6 vertebrae and between the right lobe and center of the liver. Slight variations on impact locations were used to prevent excessive impacts at any site on the torso. A total of 26 tests were conducted which included a replication of two selected cases. These test conditions and locations are detailed in Tables 2 and 3. The results from the highlighted tests are discussed in this paper.

[3]Endevco model 7270A-60K.

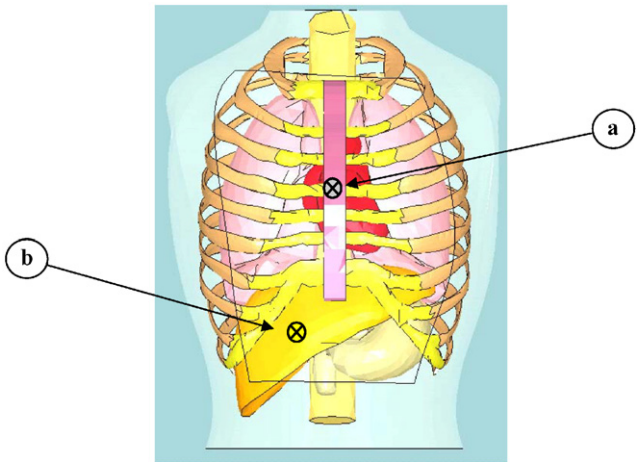

Fig. 5. Bullet impact locations: (a) at the central sternum body anterior to vertebra T6 and (b) at the central liver region between the right and left lobes of the liver.

Table 2
Test conditions for ballistic impacts to the sternum

Vest level	Shot location		
	Superior sternum body	Central sternum body	Inferior sternum body
I	×	×	×
IIa	×	×	×
II	×	×	×
IIIa	×		× ×

The superior and inferior sternum shots were located 2.5 cm above and below the central sternum location. The results from the highlighted tests are presented.

Table 3
Test conditions for ballistic impacts to the liver

Vest level	Shot location		
	Right central liver	Central liver	Left central liver
I	×	×	×
IIa	×	×	×
II	×	×	×
IIIa	×		× ×

The right and left central impact locations are located 2.54 cm to the left and right of the central impact location, respectively. The results from the highlighted tests are presented.

3. Results

The organ pressure time histories were recorded for each ballistic test conducted on the HSTM. Fig. 6 provides experimental results for organ pressure response to ballistic impact tests targeting the sternum and the liver for the Level IIIa impact conditions. The

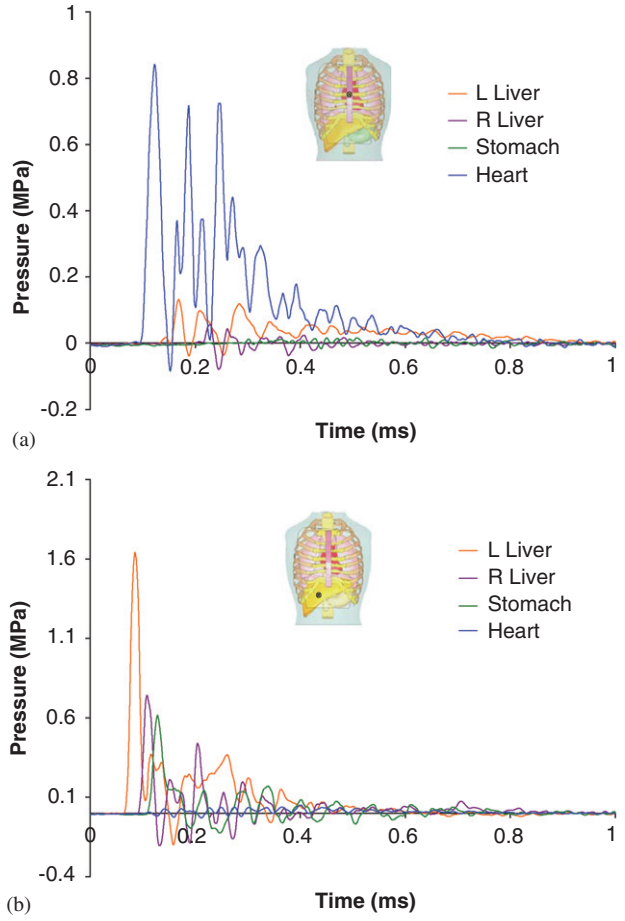

Fig. 6. Pressures in the organs following the impact of a 9 mm bullet with the Level IIIa vest and impact velocity of 430 m/s to (a) the sternum and (b) between the right and left lobes of the liver.

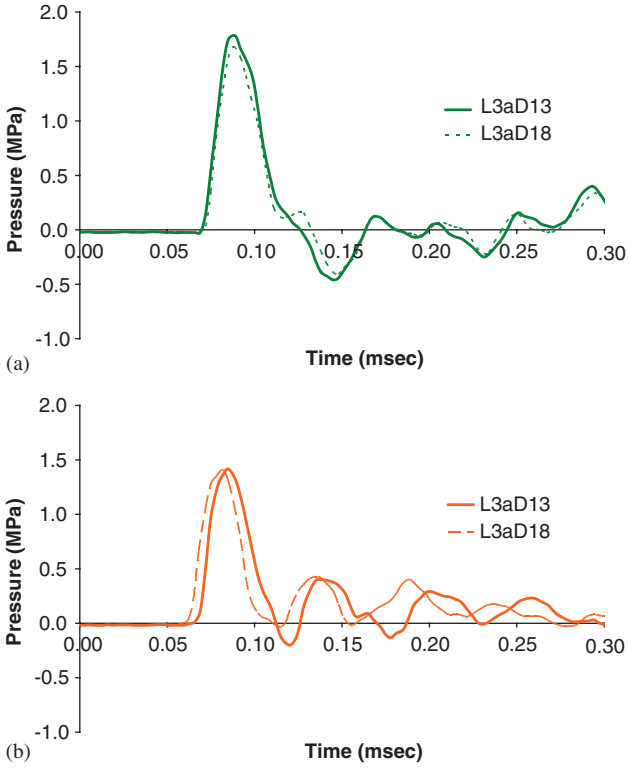

Fig. 7. The repeatability of the HSTM pressure response to a 9 mm bullet impact at 430 m/s to the left central liver for sensors located in (a) the stomach and (b) the left lobe of the liver.

organ response is characteristic of that observed for all tests with similar impact conditions. Impact to the sternum resulted in a peak pressure within the heart of approximately 0.85 MPa. The peak pressures in the organs further from the point of impact were considerably lower than that of the heart with the largest being recorded in the left lobe of the liver at 0.12 MPa. The impact of the 9 mm bullet to the central region of the liver created a peak pressure in the left lobe of the liver of 1.64 MPa. The right lobe of the liver and stomach underwent peak pressures of 0.74 and 0.62 MPa, respectively, while the sensor located in the heart recorded a pressure of 0.2 MPa. Fig. 7 illustrates the repeatability of the torso response as measured by the pressure sensors for two repeat tests for an impact to the liver under Level IIIa conditions. The repeat pressure responses for both the stomach and the left lobe of the liver have nearly identical profiles between tests with peaks that differ by 6% and 1%, respectively.

Fig. 8 shows the HTFEM response to a 9 mm bullet impacting a NIJ level IIIa soft armor vest in the middle of the sternum at a velocity of 430 m/s. The pressure response for each organ is provided in Fig. 9 as a comparison with the response of the HSTM observed experimentally. A similar comparison is provided in Fig. 10 for the HTFEM versus HSTM response for Level II conditions for an impact to the liver. The peak pressures for these tests are provided in Tables 4 and 5. An additional comparison was performed between the sternum accelerations for the HSTM and HTFEM under Level I, IIa, and II impact conditions. The results are presented graphically in Fig. 11. The peak acceleration values for both the computational and experimental models are included in Table 6. All HTFEM data traces are plotted beginning with the known time of the bullet contact with the vest. The HSTM data traces are initialized at the estimated time of bullet contact with the vest based on muzzle velocity and the distance of the barrel from the torso.

4. Discussion

The physical HSTM and computational HTFEM of a 5th percentile male were constructed to evaluate the response of the human torso to ballistic impact. Both

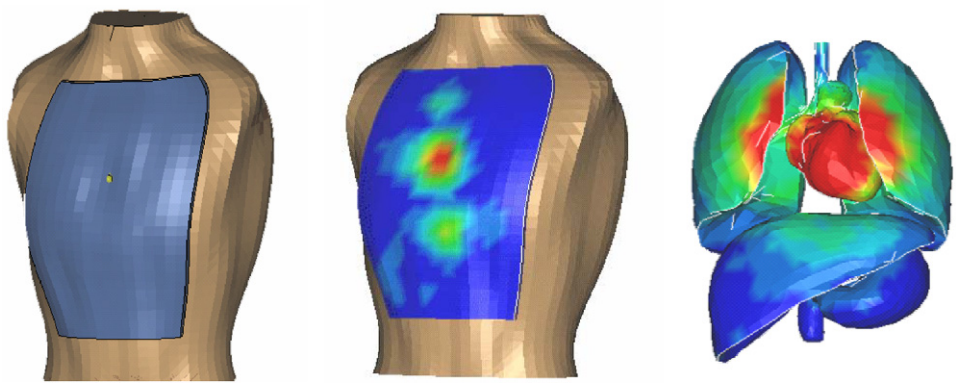

Fig. 8. Pressures response of the HTFEM and organs following simulated impact of a 9 mm projectile at a velocity of 430 m/s against a Level IIIa soft armor vest on the sternum.

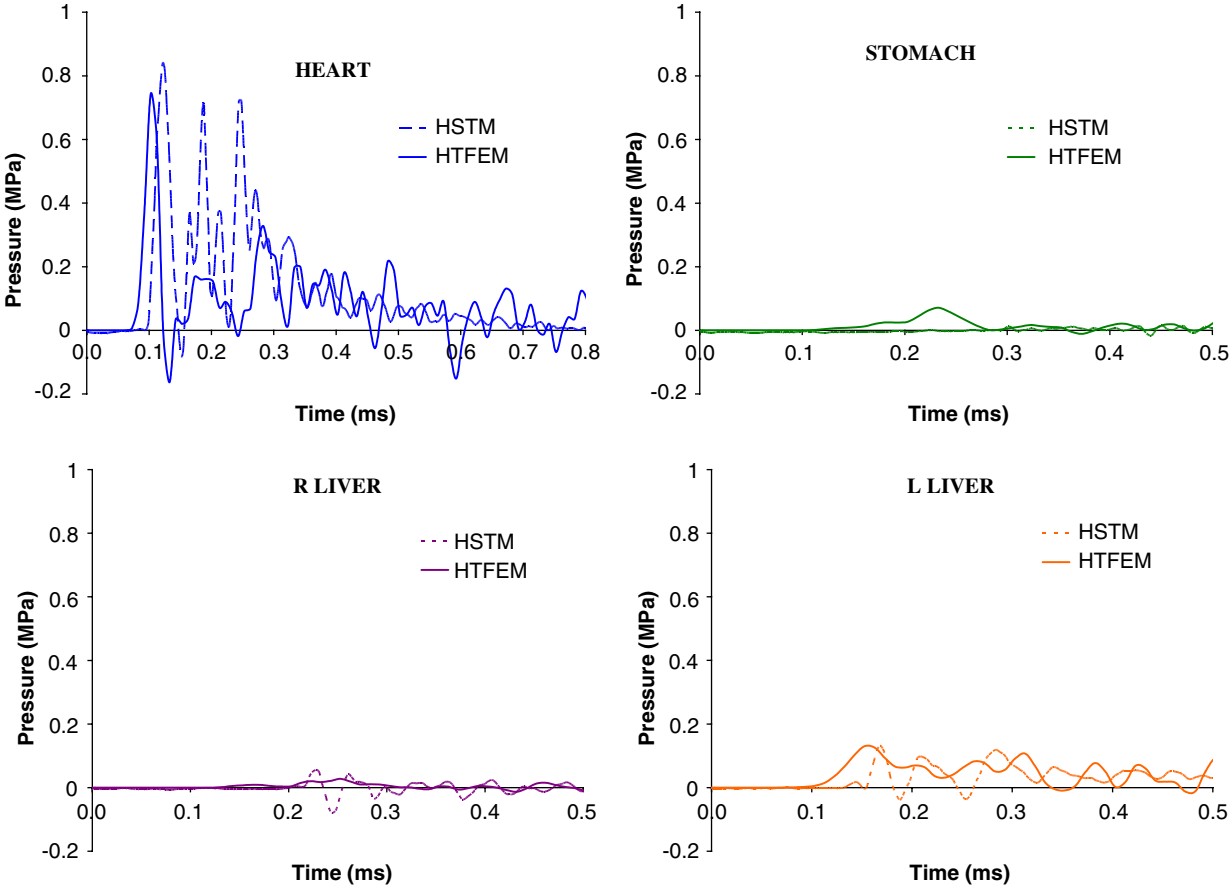

Fig. 9. A comparison of HTFEM and HSTM organ pressure for Level IIIa ballistic impact (9 mm bullet, 430 m/s) to the superior sternum body.

models were evaluated under a range of ballistic impact conditions while outfitted with a soft armor vest. Experimentally, pressure measurements were taken from sensors embedded in the organs of the HSTM and accelerations were recorded from the sternum during impact. Similarly, organ pressure measurements were taken from the HTFEM by selecting the node in the computational model that corresponded with the physical location of the sensor in the HSTM and averaging all of the pressures for the elements contacting that node. The sternal accelerations from the HTFEM were taken from the same location in which the accelerometer was attached on the physical model.

The pressure response of each organ was dependent upon the impact conditions. Fig. 6a provides the characteristic pressure responses for a 9 mm bullet

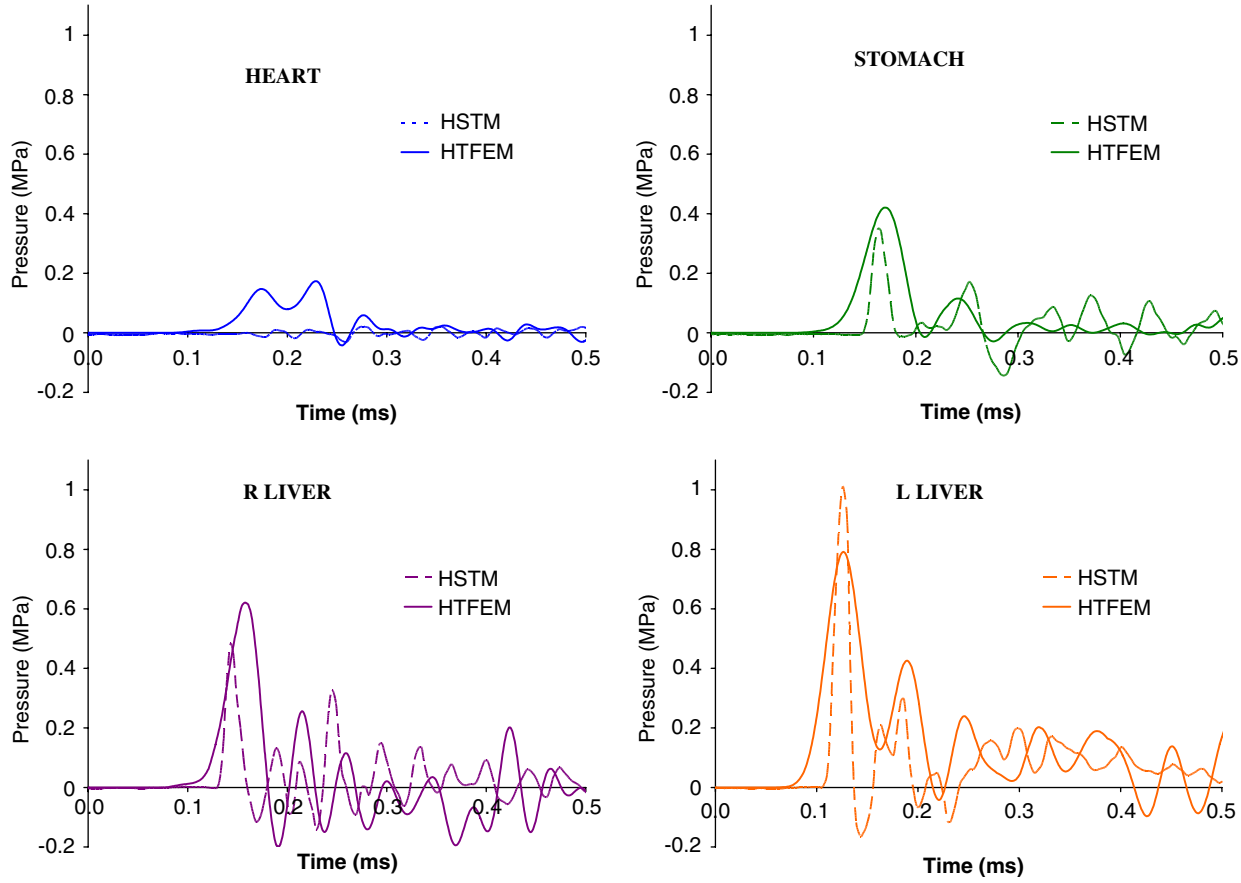

Fig. 10. A comparison of HTFEM and HSTM organ pressure for a Level II (9 mm bullet, 358 m/s) ballistic impact over the right central liver region.

Table 4
Peak organ pressures for the torso models outfitted with soft body armor due to ballistic impact to the sternum

Vest level	Target velocity (m/s)	Heart		Stomach		Liver (R Lobe)		Liver (L Lobe)	
		HTFEM (MPa)	HSTM (MPa)	HTFEM (MPa)	HSTM (MPa)	HTFEM (MPa)	HSTM (MPa)	HTFEM (MPa)	HSTM (MPa)
Level I	329	0.284	0.191	0.029	0.003	0.017	0.013	0.109	0.031
Level II	358	0.780	0.381	0.072	0.011	0.036	0.016	0.034	0.053
Level IIIa	430	0.743	0.841	0.072	0.007	0.025	0.055	0.130	0.132

Table 5
Peak organ pressures for the torso models outfitted with soft body armor due to ballistic impact to the region between the right and left lobes of the liver

Vest level	Target velocity (m/s)	Stomach		Liver (R Lobe)		Liver (L Lobe)		Heart	
		HTFEM (MPa)	HSTM (MPa)	HTFEM (MPa)	HSTM (MPa)	HTFEM (MPa)	HSTM (MPa)	HTFEM (MPa)	HSTM (MPa)
Level I	329	0.242	0.240	0.324	0.384	0.509	0.553	0.097	0.010
Level IIa	332	0.438	0.395	0.651	0.556	0.841	1.132	0.176	0.028
Level II	358	0.421	0.350	0.621	0.482	0.791	1.011	0.173	0.021

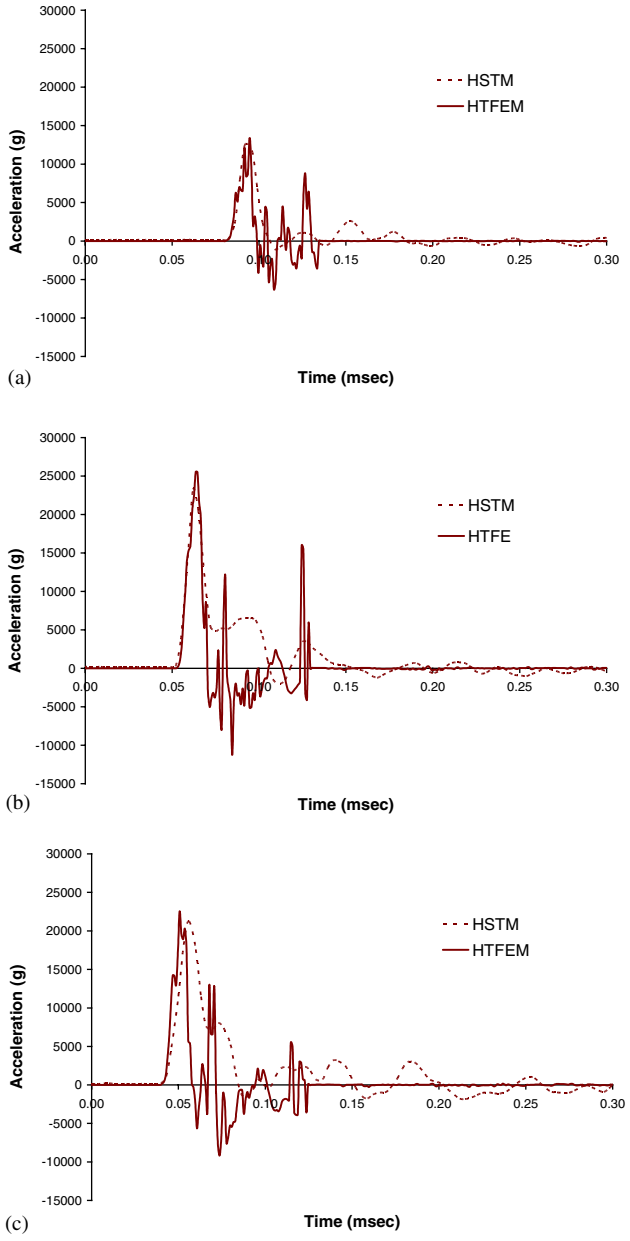

Fig. 11. Comparison of HSTM and HTFEM sternum accelerations for (a) Level I—329 m/s, (b) Level IIa—332 m/s, and (c) Level II—358 m/s. Impact location on the sternum anterior to T6.

Table 6
Comparison of the sternum accelerations during impact to the sternum for both the computational and physical models

Vest level	Target velocity (m/s)	Sternum acceleration	
		HTFEM (g)	HSTM (g)
Level I	329	13395	12553
Level IIa	358	25532	23288
Level II	430	22530	21285
Level IIIa	430	14676	5912*

*The accelerometer mount detached during this test.

impact on a Level IIIa vest at 430 m/s impact with the impact location at the sternum. The pressure experienced by the heart is much larger than that seen by the liver and stomach sensors and occurs first. This is likely due to the proximity of the organ to the location of ballistic impact. A similar response is evident in Fig. 6b for an impact on a Level IIIa vest with the impact location over the central region of the liver. The sensor located in the left lobe of the liver, closest to the point of impact, responded with the largest peak pressure followed by that recorded from the right lobe of the liver and then the stomach. The pressure response from the heart, the organ furthest from the point of impact, was much less than the pressure in the other organs.

The repeatability of these measurements was evaluated in Fig. 7. The stomach and left lobe of the liver pressure responses for two tests with similar impact conditions are provided. The pressure profiles exhibit very similar patterns and the peak pressures differ by 6% for the stomach and 1% for the left liver. This degree of repeatability existed for the heart in sternal impacts and for the stomach and liver for liver impacts. For organs further from the targeted point of impact, the same degree of repeatability was not seen. This is likely due to the directionality of the pressure sensors and the influence of lateral loading on the sensor housing.

The pressure response from the HTFEM exhibited a similar trend as the HSTM with the organ nearest the impact exhibiting the earliest and largest pressure response. The response of the HTFEM organs to Level IIIa impact conditions on the sternum are provided graphically in Fig. 9. In addition, the recorded pressures from the HSTM experimentation are plotted for comparison. The initial peak value for pressure in the heart was found to be 0.74 MPa for the HTFEM and 0.84 for the HSTM for a difference of 14%. Subsequently, it was characteristically observed that peak pressure agreement between models for locations further from the point of impact was reduced. Comparisons of the model peak pressure values for the sternal impacts are included in Table 4. In Fig. 9, the slight phase shift in the pressure traces is likely due to contributions from the method of estimating the time of bullet impact on the HSTM and any shift in original sensor position that was matched with the corresponding location in the HTFEM.

The comparison of pressure response for the organs of both models under Level II impact conditions to the liver are shown in Fig. 10. Due to the change in impact location from the sternum to the liver, the values for the liver and stomach pressures have increased significantly while the heart response has decreased. The level of agreement between computational and experimental organ pressures near the site of the impact

characteristically differed by much less than 30%. However, lesser agreement exists between models for the heart pressure when impact is over the liver. A comparison of the model peak pressure values for the liver impacts is included in Table 5.

The experimental and computational results demonstrate exceptional pressure response agreement near the point of impact when compared with locations further from the point of impact (Tables 4 and 5). One contributing factor is likely due to the design of the pressure sensors installed in the HSTM. The sensor previously described is a single-axis transducer with the sensitive axis positioned in its respective organ parallel to the transverse (horizontal) plane of the torso. This alignment places the sensitive axis for sensors near the impact in line with the primary pressure wave. However, due to sensor directionality, those sensors further from impact will detect only a portion of the pressure wave as it reaches their location and report a reduced pressure when compared with the computational model. Furthermore, lateral pressures impacting the housing of sensors further from impact can also influence the output of the sensor. Another observation evident from these results is that the pressures in organs near the impact point from both the HTFEM and HSTM were higher for impact over the soft organs (liver) than over hard tissue (bone). As would be expected, the sternum acts to absorb energy and protect the organs from injury, which is demonstrated by these results.

The HSTM sternal accelerations were recorded for impacts to the sternum under Level I, IIa, and II conditions and compared to the output of the HTFEM in Fig. 11. The acceleration profiles show excellent agreement and the peak accelerations were within 10% between models. The sternal accelerations varied due to test conditions with the lowest acceleration occurring for the Level I conditions of a 22 caliber (2.6 g) bullet impacting at 329 m/s. Although the impact kinetic energy is 20% greater for the Level II condition, the HSTM Level IIa peak acceleration is slightly greater in magnitude than the Level II response. This is possibly due to the contribution of the soft armor vest thickness in reducing sternal accelerations. The thickness for the Level II condition is 9.50 mm compared with 7.88 mm for Level IIa.

Limited data exists in the literature with which to compare the pressure and acceleration response of a torso under similar impact conditions. Raftenberg (2003) did conduct ballistic tests on PMHS outfitted with soft body armor and compare with a FEM of the human torso. The impact velocities for a 9 mm bullet ranged from 425 to 448 m/s and the resulting peak accelerations of the sternum were between 2300 and 5100g. Depending on FEM parameters, Raftenberg found between 19% and 82% difference in peak accelerations when comparing the FEM and experimental PMHS results. The accelerations in the current study for the HSTM and HTFEM were approximately 20,000g under similar impact conditions. There are a number of possible explanations for the discrepancy. The HTFEM in the current study has a much finer mesh (~245,000 solid and shell elements) and uses a viscoelastic material model that includes a short-term shear modulus and bulk modulus supplied from high-rate testing of the biosimulant gels used in the HSTM, which are not the same as those in the PMHS. The FEM employed by Raftenberg had approximately 15,000 solid and shell elements and used a material model that was isotropic and rate dependent. The hexahedral elements in this FEM model were less stiff than the tetrahedral elements in the current study and could contribute to the difference in accelerations. In addition, the sensor location and fixation techniques were quite different and could contribute to differences in recorded response.

The HSTM and HTFEM evaluated in this study require further comparison with planned testing of animals and PMHS for complete model validation. However, the current efforts to develop both a physical and computational thoracic model provide comparative techniques for determining the response of the torso to ballistic impact. Due to the anatomically identical geometries and use of high-strain rate biosimulant properties, the HTFEM and HSTM show extremely similar responses in the vicinity of ballistic impact. Once these models have been fully validated, they could be used for evaluating the design and efficacy of soft body armor, determining injury mechanisms and assisting with injury prevention.

Acknowledgments

The authors would like to express their appreciation to the Office of Naval Research (ONR) under contract no. N00024-98-D-8124 for funding this work. The authors would also like to acknowledge Gary Peck, Robert Wright and Antonio Munoz for creation of the RP models, skeleton and organ molds and final assembly of the HSTM.

References

Caruso, K.S., Hijuelos, P.J., Biermann, P.J., Roberts, J.C., 2006. Development of synthetic cortical bone for ballistic and blast testing. Journal of Advanced Materials, in press.

Chen, P.H., 1973. Dynamic response of the human thoracic skeletal system to chest impact. Ph.D. Dissertation, University of California, Los Angeles.

Chen, P.H., 1978. Finite element dynamic structural model of the human thorax for chest impact response and injury studies. Aviation Space and Environmental Medicine 143–149.

Chen, P.H., Roberts, S.B., 1974. Dynamic response of the human thoracic skeleton to impact. ENG-0274, School of Engineering and Applied Science, University of California, Los Angeles.

Duck, F.A., 1990. Physical Properties of Tissue. Academic Press, Harcourt Brace Jovanovich Publishers, London.

Grosberg, P., 1969. In: Hearle, J.W.S., Grosberg, P., Backer, S. (Eds.), The Tensile Properties of Woven Fabrics—Structural Mechanics of Fibers, Yarns and Fabrics 1. Wiley-Interscience, New York, pp. 339–354.

Johnson, G.R., Beissel, S.R., Cunniff, P.M., 1999. A computational model for fabrics subjected to ballistic impact. In: Reinecke, W.G. (Ed.), Proceedings of the 18th International Symposium on Ballistics, vol. 2. Technomic Publishing, Lancaster, PA, pp. 962–969.

Jolly, J.E., Young, K.W., 2000. Computer modeling and simulation of bullet impact to the human thorax. NPS-ME-00-002, Naval Postgraduate School, Monterey, CA, June.

Jönsson, A., Clemedson, C.J., Arevbo, E., 1981. An anthropometric dummy for blast research. Proceedings of the 1983 International Conference on Protective Clothing Systems, Stockholm, Sweden, August, pp. 89–97.

Jönsson, A., Arvebo, A., Schantz, B., 1988. Intrathoracic pressure variations in an anthropometric dummy exposed to air blast, blunt impact and missiles. In: Proceedings of the Fifth Symposium on Wound Ballistics 28 (1), S125–S131.

Lyons, D.H., Patton, B.J., Bir, C.A., 1999. Injury evaluation techniques for non-lethal kinetic energy munitions. Army Research Laboratory, ARL-TR-1868.

Plank, G.R., Eppinger, R.H., 1991. An improved finite element model of the human thorax. Proceedings of the 13th ESV, pp. 902–907.

Plank, G.R., Kleinberger, M., Eppinger, R.H., 1998. Finite element modeling and analysis of thorax/restraint system interaction. In: Proceedings of the 42nd STAPP Car Crash Conference, SAE-P337, pp. 317–329.

Raftenberg, M.N., 2003. Response of the wayne state thorax model with fabric vest to a 9-mm bullet. Army Research Laboratory, ARL-TR-2897, Aberdeen Proving Ground, Aberdeen, MD, January.

Roberts, J.C., Ward, E.E., O'Connor, J.V., 2005. Modeling the effect of non-penetrating ballistic impact as a means of detecting behind armor blunt trauma. Journal of Trauma 58 (6), 1241–1251.

Roberts, S.B., Chen, P.H., 1970. Elastostatic analysis of the human thoracic skeleton. Journal of Biomechanics 3, 527–545.

Saraf, H., Ramesh, K.T., Lennon, A.M., Merkle, A.C., Roberts, J.C., 2005. Mechanical properties of soft human tissues under dynamic loading. Journal of Biomechanics, submitted.

Stuhmiller, J.H., Chuong, Phillips, Y.Y., Dodd, K.T., 1988. Computer modeling of thoracic response to blast. Journal of Trauma 28 (1), S132–S139.

Sundaram, S.H., Feng, C.C., 1977. Finite element analysis of the human thorax. Journal of Biomechanics 10, 505–516.

Wang, H.C., 1995. Development of a side impact finite element human thoracic model. Ph.D. Thesis, Wayne State University, Detroit, MI.